Cure Behavior of Paper–Phenolic Composite Systems: Kinetic Modeling

ERDOGAN KIRAN* and RAJAN IYER

Department of Chemical Engineering, University of Maine, Orono, Maine 04469

SYNOPSIS

Cure reactions in paper–phenolic composite systems were studied by differential scanning calorimetry. A phenomenological approach was used to characterize the cure kinetics. Various kinetic models including homogeneous reaction, diffusion-controlled reactions, surface reaction and phase boundary movement, and nucleation and growth-type kinetic models have been tested. Kinetic analyses using integral and derivative procedures on dynamic and isothermal data indicate that the cure reaction data can be described well with the homogeneous first-order reaction model or the Jander three-dimensional diffusion model. The activation energies are found to be in the range 20–40 kJ/mol. © 1994 John Wiley & Sons, Inc.

INTRODUCTION

Paper–phenolic composites such as laminates are manufactured by curing papers impregnated with phenolic thermosetting resins. Understanding the cure behavior and the cure kinetics is an important area of research for the manufacture of such composite materials.

Even though there is extensive literature on cure reactions and kinetics of epoxy systems and their composites with specialty fibers,[1-3] literature on the phenomenological and kinetic aspects of the curing of phenolic systems and those containing cellulosic fibers is limited.[3-10] We have recently[7] conducted a critical evaluation of procedures to study the cure process and to determine the heat of cure and conversion as a function of time or temperature in paper–phenolic composite systems. We now focus on the kinetic modeling of these reactions using differential scanning calorimetry.

Differential scanning calorimetry is often used to study cure reactions under isothermal or dynamic (nonisothermal) modes.[3] To evaluate the kinetic parameters, in the isothermal mode, experiments must be conducted at different temperatures. The attractive feature of isothermal experiments is that the rate constant at each temperature is better defined and the determination of the rate constants at different temperatures would permit the determination of the activation energy associated with the cure reactions. However, the nature of the reactions and the final products may differ at different temperatures, and the kinetic parameters thus obtained are not without ambiguity. Since numerous reactions occur simultaneously, the activation energies must be regarded as the "apparent" activation energies.

Dynamic experiments, conducted at a specified heating rate, yield conversion–time–temperature data that are comprehensive enough to permit direct evaluations of the kinetic parameters. A single dynamic run gives as much information as do several isothermal runs. Furthermore, dynamic measurements can provide kinetic information over a larger temperature range and there is no precure problems as is the case with isothermal experiments in which the sample must be first heated to the isothermal hold temperature during which cure reactions may take place.[7] In this study, both isothermal and dynamic experiments have been conducted and the results from both types of measurements have been compared.

Different methodologies have been used in the literature for the evaluation of kinetic parameters.[3,11-14] In general, kinetic expressions may be phenomenological or mechanistic. Phenomenolog-

* To whom correspondence should be addressed.

Journal of Applied Polymer Science, Vol. 51, 353–364 (1994)
 CCC 0021-8995/94/020353-12

ical models relate to the main features of the reaction kinetics and do not take into account individual reactions, whereas mechanistic models are obtained from balances of species involved in the reaction.

The phenomenological approach has been preferred in this study because the curing process is so complex that it is very difficult to identify each and every reaction. The phenomenological reaction rate can be expressed either in the differential form:

$$\frac{d\alpha}{dt} = kf(\alpha) \tag{1}$$

or in the integrated form:

$$g(\alpha) = \int \frac{d\alpha}{f(\alpha)} = \int k\,dt \tag{2}$$

where α is the fractional conversion at any time t; k, the Arrhenius rate constant, and $f(\alpha)$, a functional form of α that depends on the reaction mechanism.

The methodology of evaluating fractional conversions is described in the preceding paper.[7] They are determined from the ratio of the partial to total peak areas (representing partial and total heat of cure) associated with the cure reaction.

Functional forms of $f(\alpha)$ representing different reaction mechanisms have been described in the literature[3,12] and the ones tested in the present study are shown in Table I. Table I includes homogeneous reaction models, autocatalytic reaction models, phase boundary movement (or surface reaction) models, and nucleation and growth models. In the

Table I Kinetic Models Evaluated; Rate = $kf(\alpha)$

Model	$f(\alpha)$	$g(\alpha) = \int \frac{d\alpha}{f(\alpha)}$
Homogeneous reaction models		
First order	$(1-\alpha)$	$-\ln(1-\alpha)$
nth order	$(1-\alpha)^n$	$\frac{[1-(1-\alpha)^{(1-n)}]}{(1-n)}$
Autocatalytic reaction		
$m = 1, n = 1$	$\alpha^m(1-\alpha)^n$	$\ln[\alpha/(1-\alpha)]$
$m = 2, n = 1$		$\ln[\alpha/(1-\alpha)] - 1/\alpha$
$m = 2, n = 2$		$2\ln[\alpha/(1-\alpha)] + 1/(1-\alpha) - 1/\alpha$
Reaction interface models (phase boundary movement models)		
Diffusion Controlling		
One-dimensional diffusion where		
$n = 1/4; 1/3; 1/2; 2$	$\frac{1}{n}\alpha^{(1-n)}$	α^n
Two-dimensional diffusion	$\frac{-1}{\ln(1-\alpha)}$	$(1-\alpha)\ln(1-\alpha) + \alpha$
Three-dimensional diffusion		
Jander kinetics	$\frac{3(1-\alpha)^{2/3}}{2[1-(1-\alpha)^{1/3}]}$	$[1-(1-\alpha)^{1/3}]^2$
Gintsling–Brounshtein kinetics	$(3/2)[(1-\alpha)^{-1/3} - 1]$	$1 - 2/3\alpha - (1-\alpha)^{2/3}$
Surface reaction controlling		
Contracting geometry $n = 2; 3$	$n(1-\alpha)\frac{(n-1)}{n}$	$1-(1-\alpha)^{1/n}$
Nucleation and growth models		
Random nucleation	α	$\ln\alpha$
Avrami-Erofeev kinetics with, $n = 1; 1.5; 2; 3; 4$	$n(1-\alpha)[-\ln(1-\alpha)]^{(1-1/n)}$	$[-\ln(1-\alpha)]^{1/n}$

table, for each model, in addition to the form of $f(\alpha)$, the integrated form, $g(\alpha)$ is also included.

Applicability of a model can be tested using either derivative [eq. (1)] or the integral form [eq. (2)] of the rate expressions. Both approaches have been evaluated in the present study to determine the validity of a mechanism and the consistency of the rate constants and activation energies.

EXPERIMENTAL

Samples

Phenolic resin-impregnated Kraft paper composites were prepared using a generic phenol–formaldehyde resin in methanol–water solutions. The resin content of the composites were 27% by weight.

Differential Scanning Calorimetry

A Perkin-Elmer DSC-2 differential scanning calorimeter digitized in our laboratory[10,15] for data collection and analysis has been used in all experiments.

With this system, heats of transitions are determined with an accuracy better than ±2.5%. Procedures for the determination of peak areas, heats of transformations, and fractional conversions are described elsewhere.[7,15] In all experiments, stainless-steel large-volume capsules were used to suppress liberation of volatiles and prevent loss of mass. These capsules are capable of withstanding pressures up to 350 psi (2.4 MPa), which in the present study limited the experiments to temperatures below 525 K.

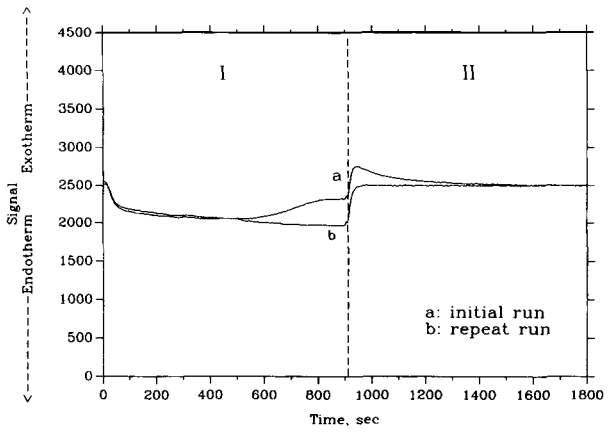

Figure 1 Isothermal run on composite at 450 K (10 K/min approach). Sample weight normalized to 7.5 mg. Region I, dynamic heating range; Region II, isothermal hold range.

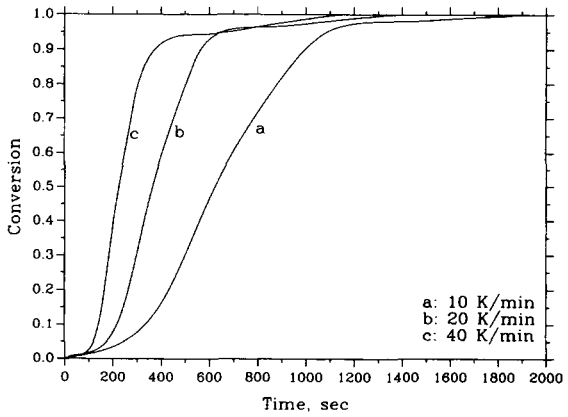

Figure 2 Comparative conversion profiles obtained from dynamic scans conducted at 10, 20, and 40 K/min heating rates.

Heating Modes

Experiments were conducted either under dynamic heating modes of 10, 20, and 40 K/min up to 520 K or isothermally at 430, 440, 450, 460, and 470 K. In isothermal experiments, the effect of different heating rates (i.e., 10, 20, 40 K/min) to reach the selected isothermal hold temperatures were evaluated.

RESULTS AND DISCUSSION

Fractional Conversions

Figure 1 shows a typical DSC scan obtained by heating the sample at 10 K/min up to 450 K and then holding isothermally thereafter. The scan a in the figure shows the exotherm associated with the cure process in the dynamic heating range and the decaying signal in the isothermal hold range. The base line is obtained by repeating the DSC scan after cure reactions have been completed. The total area between the initial and final scans provide the needed information to calculate the heat of cure[7] and the partial areas corresponding to different time during cure provide the needed information to calculate fractional conversions.

Figure 2 shows the fractional conversion data obtained from dynamic experiments conducted at 10, 20, and 40 K/min heating rates in the temperature range of 350–520 K. All the samples were held isothermally for 15 min after reaching 520 K to ensure complete cure.[7] As expected, to achieve the same degree of conversion requires a longer time in slower heating modes.

Figure 3 shows the fractional conversion data obtained from isothermal experiments conducted at 435, 440, 450, and 470 K. In all these experiments, the isothermal hold temperatures were approached at 10 K/min.

Figure 4 shows the fractional conversion in isothermal experiments conducted at 450 K but approached at different heating rates. To achieve the same degree of conversion requires a longer time under the slower approach to hold the temperature.

Kinetic Modeling

Kinetic modeling has been carried out in a series of steps. As stated earlier, kinetic modeling can be performed using both derivative or integral procedures. If the derivative mode of analyses is used, then kinetic modeling starts with eq. (1). If the integral mode of analyses is used, then kinetic modeling starts with eq. (2). After choosing the mode of analysis, for the kinetic model to be tested, the functional form $f(\alpha)$ is selected from Table I. Then, the experimental conversion–time data is used to test the model. The testing criteria are high regression coefficients and adherence to intercept requirements. A successful model should describe the experimental data irrespective of the mode of analysis. Procedures and results of the analyses are presented in the following sections. These procedures and computer software have been all tested and verified with simulated conversion–time data for different models.

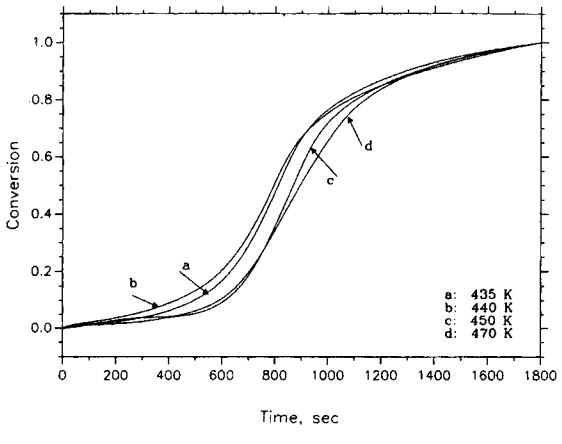

Figure 3 Comparative conversion profiles obtained from isothermal scans conducted at 430, 440, 450, 460, and 470 K with 10 K/min approach to the isothermal temperature.

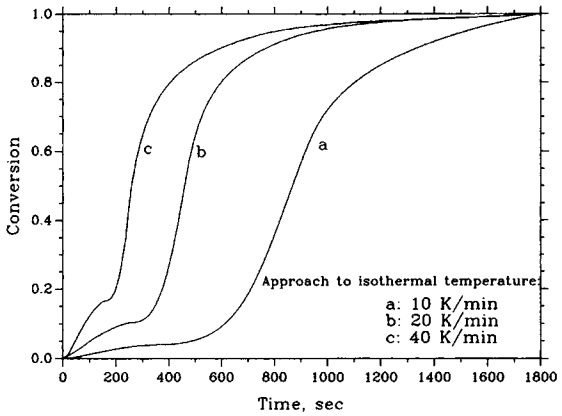

Figure 4 Comparative conversion profiles obtained from isothermal scans conducted at 450 K at 10, 20, and 40 K/min approach to hold temperature.

Modeling Using Conversion Data from Dynamic Experiments

Derivative Method of Analysis

By incorporating the Arrhenius form of the rate constant k, i.e.,

$$k = A \exp(-E/RT),$$

eq. (1) can be modified as

$$\frac{d\alpha/dt}{f(\alpha)} = A \exp\left(\frac{-E}{RT}\right) \tag{3}$$

where A is the frequency factor; E, the activation energy; R, the gas constant; and T, the temperature in K.

Taking the logarithm of both sides, we get

$$\ln \frac{d\alpha/dt}{f(\alpha)} = \ln A - \frac{E}{RT} \tag{4}$$

which forms the starting equation for the derivative analysis of the dynamic data. The computer program reads in the dynamic data from the data file and calculates $\ln\{(d\alpha/dt)/[f(\alpha)]\}$ for each conversion point using the functional form for the chosen model. A plot of the left-hand side of the above equation against $1/T$ should give a straight line with a slope of $-E/R$ for the correct functional form $f(\alpha)$. The intercept is $\ln A$ from which the frequency factor can be evaluated.

Integral Method of Analysis

Equation (1), after including the Arrhenius form of the rate constant and rearrangement, can be integrated up to a certain conversion α corresponding to a time t:

$$\int_0^{\alpha} \frac{d\alpha}{f(\alpha)} = A \int_0^{t} \exp\left(\frac{-E}{RT}\right) dt \qquad (5)$$

This integration is carried out numerically with an appropriate computer program. For common kinetic models, the left-hand side can be integrated analytically, and these are given as $g(\alpha)$ functions in Table I. Therefore, eq. (5) can be written as

$$g(\alpha) - g(0) = A[Z(t) - Z(0)] \qquad (6)$$

where

$$Z(t) = \int_0^{t} \exp\left(\frac{-E}{RT}\right) dt$$

A computer program reads the conversion–temperature–time data and uses it to carry out the analysis for the selected kinetic model. The software calculates $g(\alpha) - g(0)$ and stores it in an array. An initial guess for the activation energy is made that is numerically corrected until a satisfactory solution is obtained. The program starts with an initial guess for the interval of E/R and curve fits for the chosen kinetic model.

The initial guess for E/R need not be close to the actual value. The program decides whether the upper limit of the chosen interval is too high, which would mean excessive iterations and slower convergence to the actual value, or the lower limit of the chosen interval is too low and there is no possibility of convergence to the actual value. The check used in the software is the linear regression coefficient. The initial interval for E/R ($e1 \leq E/R \leq e2$) is divided into three equal intervals and the regression coefficient is calculated at $e1$, $em = (e1 + e2)/2$, and $e2$. The corresponding linear regression coefficients are $r1$, rm, and $r2$. If $r2 > rm > r1$, then the upper limit of the range is extended to a higher value. If $r2 < rm < r1$, then a lower limit of the range is extended to a smaller value. When rm is greater than $r2$ and $r1$, then we have the appropriate range for E/R. The program now concentrates on converging to the best value of E/R in this interval. This interval is further divided into 10 equal parts. The actual value lies inside one of these intervals. The software finds the best regression coefficient among the 10 subintervals. The search is continued by dividing the interval with the best regression coefficient into further 10 subdivisions. This process of convergence is repeated until a specified criteria is satisfied. In the present study, the difference between $e1$ and $e2$ were specified to be less than 10^{-7}, which would indicate that we have arrived at E/R with the best regression coefficient fitting the model.

Modeling Using Conversion Data from Isothermal Experiments

Derivative Method of Analysis

As in the case of analyzing dynamic data, the starting equation for derivative analysis of isothermal data is eq. (1). The computer program calculates $(d\alpha)/(dt)$ by finding the slope between two adjacent conversion points in the isothermal data. Then, for the selected model, it calculates the value of $f(\alpha)$ at each point and stores the results in an array. A plot of $(d\alpha)/(dt)$ with $f(\alpha)$ should yield a straight line with a slope k and zero intercept.

Integral Method of Analysis

For isothermal reactions with the temperature being constant, eq. (2) can be integrated to

$$\int_0^{\alpha} \frac{d\alpha}{f(\alpha)} = k \int_0^{t} dt \qquad (7)$$

or

$$g(\alpha) - g(0) = kt \qquad (8)$$

Since in isothermal experiments there is an initial dynamic portion, during which some reaction may take place, the start of the actual isothermal conditions corresponds to a nonzero value of conversion, α_1. With this consideration, eq. (8) becomes

$$g(\alpha) - g(\alpha_1) = kt_{iso} \qquad (9)$$

where t_{iso} represents the time for the isothermal part of the experiment. A plot of $g(\alpha) - g(\alpha_1)$ vs. t_{iso} should be a straight line with zero intercept and a slope equal to the rate constant k.

Kinetic Models

The models tested during the present study represent a wide variety of reaction mechanisms, the simplest being the homogeneous reaction model which assumes that the reaction is occurring si-

multaneously at the molecular level throughout the sample. This may be a rather simplistic assumption considering the complexity of cure reactions. However, it establishes a reference for comparative analyses. Also included in the homogeneous reaction mechanism category is the autocatalytic type of reactions, where the initial reaction products help catalyze the reaction process, thus accelerating the reaction rate. Autocatalytic reaction models are often used to describe the cure kinetics in epoxy systems.[1-3,16]

When the initiation of reaction occurs at a phase boundary and advances into the unreacted zone of the sample, the kinetic characteristics of the overall rate process are determined by the geometrical mode of advance of the reaction interface from these boundaries toward the centers of the unreacted zone. Depending on whether this advance (phase boundary movement) occurs in two or three dimensions, the rate expressions are termed contracting area or contracting volume equations, respectively.[11,12,17]

In diffusion-limited reactions, the overall rate is determined by the movement of reactant species toward, or a product from, a reaction interface. Diffusion can be envisioned to take place in one, two, or three dimensions. The rate expressions include these differences in the mode of diffusion. In the 3-dimensional diffusion models tested in this study, the Gintsling–Brounshtein model assumes Fick's law of diffusion while the Jander model assumes that the thickness (x) of the diffusion layer increases according to $dx/dt = D/x$, where D is the diffusivity and t denotes the time.[18]

The nucleation process involves conversion of a small volume of reactant into a stable particle of product and continued reaction (growth) occurs preferentially at the interfacial zone of contact between these two phases. Initial nucleation and growth expressions, like the power law expression which assumes that growth rate increases continually were developed to describe crystallization processes and fail to describe actual chemical reaction processes for which such an assumption would be unrealistic. However, modifications by Avrami,[19] Erofeev and Mitskevich,[20] and Mampel[21] yield a more general form of the equation that is found to describe many reactive systems over the entire conversion range.

Results of Kinetic Modeling Using Data from Dynamic Experiments

Derivative Method of Analysis

Homogeneous models are often used to describe cure reactions in the literature.[6,22,23] Figure 5 is a plot for

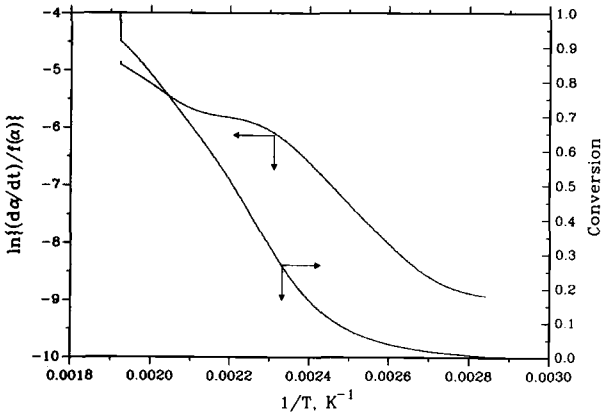

Figure 5 Derivative analysis of dynamic data obtained at 10 K/min heating rate. Homogeneous first-order kinetics model.

the derivative analysis of the dynamic data using the homogeneous first-order kinetics model. The plot shows the variation of $\ln\{(d\alpha/dt)/[f(\alpha)]\}$ with $1/T$ and the corresponding conversions. The $\ln\{(d\alpha/dt)/[f(\alpha)]\}$ vs. $1/T$ plot is not a straight line over the whole $1/T$ range and shows a marked change in slope at around 30% conversion. Similar results were obtained from the analyses of dynamic data collected at 20 and 40 K/min heating rates. The change in slope occurred at around 30% conversion in these runs also. Since the slope is a measure of the activation energy, the results indicate a marked change in the energetics of the reaction beyond 30% conversion. As shown in Table II(a), the activation energy becomes approximately one-half its value observed at the lower conversion range. Such a decrease in apparent activation energy is commonly observed in heterogeneous reactions, especially when diffusional limitations set in.[24] The present results may therefore be interpreted to imply that beyond 30% conversion diffusional factors become significant in curing of phenolic–paper composites. It is interesting to note that the rate at which 30% conversion is reached does not seem to matter, and the shape of the plots show the change at this characteristic conversion.

To better describe the data, further analyses were carried out separately in the conversion ranges of 0–30% and 30–95%. As shown in Figure 6, the homogeneous first-order reaction model describes the conversion data up to 30% conversion well, and the plots of the $\ln\{(d\alpha/dt)/[f(\alpha)]\}$ vs. $1/T$ is indeed a straight line. In this conversion range, we have tested all other models shown in Table I. The homogeneous first-order model was found to describe the data best.

Table II Derivative Analyses of Dynamic Data

Model	r^a	E/R	A
(a)			
First-order kinetics (0–30% converion range)	−0.93467	4500	49
Jander kinetics models (0–30% conversion range)	−0.89063	9500	1.5×10^5
First-order kinetics (30–95% conversion range)	−0.99999	2600	1
Jander kinetics model (30–95% conversion range)	−0.99999	3800	1
(b) 0–95% conversion range			
First-order kinetics	−0.9740	4,500	41
Autocatalyzed kinetics model			
$n = 1, m = 1$	0.4121	−700	0.0015
$n = 1, m = 2$	0.8485	−5900	5.7×10^{-8}
$n = 2, m = 2$	0.6544	−3500	2.7×10^{-5}
1-Dimensional diffusion model ($n = 2$)	−0.8965	7200	4,300
2-Dimensional diffussion model ($n = 2$)	−0.9292	8200	31,200
Jander kinetics	−0.9562	9500	1.9×10^5
Gintsling-Brounshtein model	0.8381	−4500	1.5×10^{-7}
Contracting geometry model			
$n = 2$	−0.9233	3300	1.0
$n = 3$	−0.9523	3700	2.0
Random nucleation kinetics model	0.8049	−3000	3.2×10^{-6}
Avrami-Erofeev model			
$n = 1.5$	−0.9529	2400	0.4
$n = 2$	−0.8371	1400	0.04
$n = 3$	−0.3162	400	0.003
$n = 4$	0.0676	−90	0.0008

E: activation energy, r: linear regression coefficient, A: frequency factor.
[a] The negative value of the regression coefficient is due to the negative slope of the line in eq. (4).

In the conversion range 30–95%, not only the homogeneous first-order model but also a diffusional model (the Jander model) were found to fit the data well. Figure 7 shows the results for this model. The fact that this model, which is not as good below 30% conversion [see Table II(a)], yet describes the data so well above 30% conversion, is consistent with the above-mentioned observation that the apparent ac-

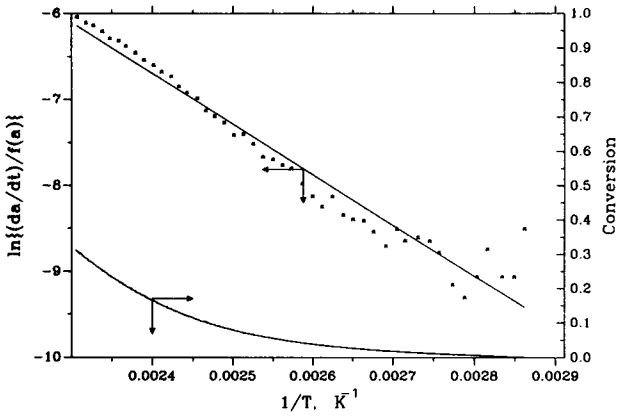

Figure 6 Derivative analysis of dynamic data obtained at 10 K/min heating rate. Homogeneous first-order kinetics model. Conversion range 0–30%.

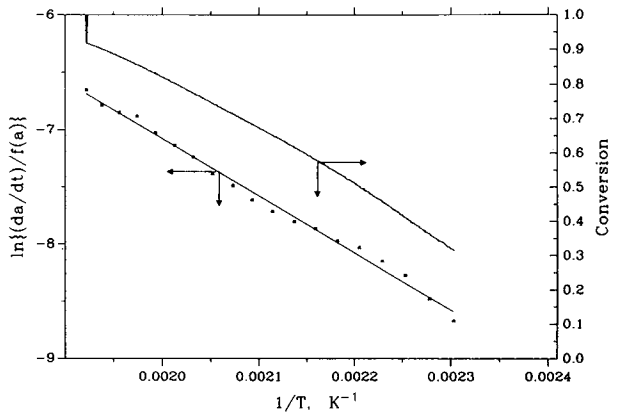

Figure 7 Derivative analysis of dynamic data obtained at 10 K/min heating rate. Jander kinetics model. Conversion range 30–95%.

tivation energies decrease beyond this conversion and mass transfer limitations set in. Among the diffusional models, the Jander model has been found to best describe the data.

The results from using all the models including first-order and Jander are shown in Table II(b) for the total conversion range of 0–95%. For comparison, the results for the homogeneous first-order and the Jander models are also included in the table for this conversion range. Over the total range, none of the models perform well, but first-order and Jander are still better than the others. Even though not reported here, for other models, analysis over narrower conversion ranges did not give results better than did the homogeneous first-order or Jander model.

Integral Method of Analysis

For integral analyses, the main criteria are that the linear regression coefficient should be very close to 1 and the intercept should be very close to zero. This follows from eq. (2). Continuing with our results from derivative analyses of the dynamic data, integral analyses were performed separately on two conversion ranges, namely, 0–30% and 30–95%. Initially, the homogeneous first-order model was tested for the experimental data. Figure 8 shows the results for the homogeneous first-order model in the conversion range 0–30%. The dots represent the experimental data and the solid line represents the model prediction. The conversions are also shown on the right axis. As can be seen, the data lie on the straight line predicted by the model, showing a very good fit of the model to experimental data. The first-order homogeneous and the Jander kinetics models were also fitted to the conversion data in the range 30–95%. Figures 9 and 10 show the results of these analyses. Once again, these models describe the data well.

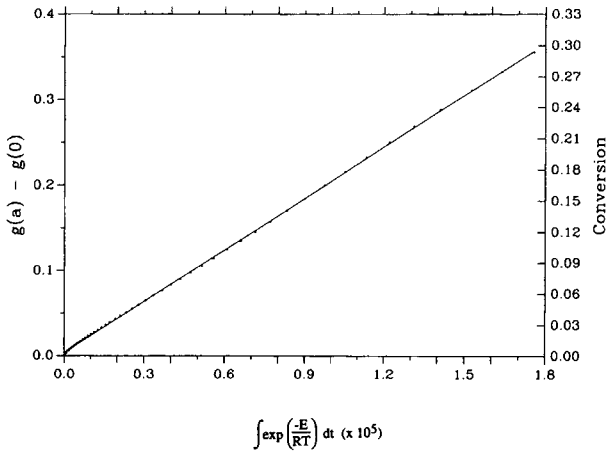

Figure 8 Integral analysis of dynamic data obtained at 10 K/min. Homogeneous first-order kinetics model. Conversion range 0–30%. (Values on the left vertical axis correspond to the conversion values on the right vertical axis.)

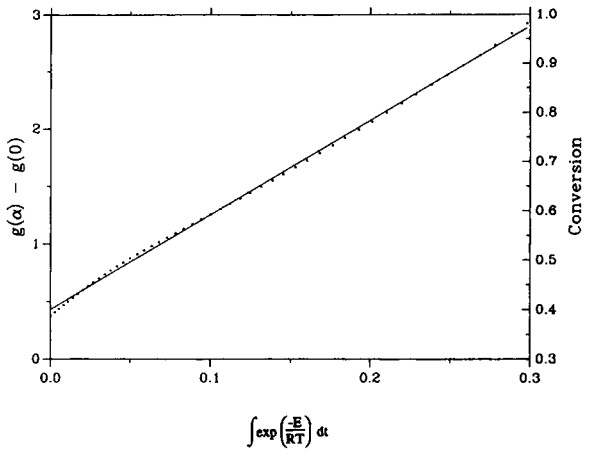

Figure 9 Integral analysis of dynamic data obtained at 10 K/min. Homogeneous first-order kinetics model. Conversion range 30–95%.

Table III(a) shows the activation energies calculated for the first-order homogeneous and Jander diffusion models. The activation energy for the higher conversion range is approximately $\frac{1}{2}$ of the activation energy calculated for the lower conversion range, indicating again the presence of mass-transfer limitations at high conversions.

Table III(b) shows the parameters calculated with the other models, for the whole conversion range 0–95%. They do not show a good fit to exper-

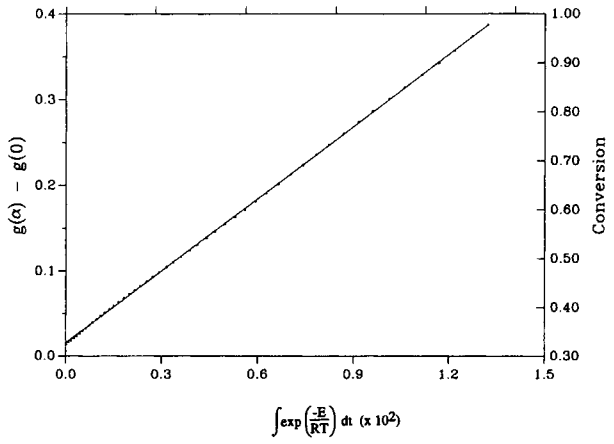

Figure 10 Integral analysis of dynamic data obtained at 10 K/min. Jander kinetics model. Conversion range 30–95%.

Table III Integral Analyses of Dynamic Data

Model	E/R	r	i	A
	(a)			
First-order kinetics (0–30% conversion range)	6,900	0.9999	3.9×10^{-3}	2000
Jander kinetics (0–30% conversion range)	14,000	0.9994	-1.2×10^{-5}	2.1×10^{10}
First-order kinetics (30–95% conversion range)	3,700	0.9995	0.4	8
Jander kinetics model (30–95% conversion range)	5,200	0.9999	1.5×10^{-2}	26
	(b) 0–95% conversion range			
First-order kinetics	3,500	0.9993	-4.7×10^{-2}	6
Autocatalyzed kinetics model $n = 2$, $m = 2$	−1,100	0.9962	−5.7	6.0×10^{-4}
1-Dimensional diffusion model ($n = 2$)	2,700	0.9914	-5.7×10^{-2}	0.5
2-Dimensional diffusion model ($n = 2$)	3,700	0.9960	-3.1×10^{-2}	3
Jander kinetics	5,700	0.9994	-5.2×10^{-3}	75
Gintsling–Brounshtein model	4,300	0.9977	-6.5×10^{-3}	2.8
Contracting geometry model				
$n = 2$	1,900	0.9960	-4.1×10^{-2}	0.05
$n = 3$	2,300	0.9976	-2.5×10^{-2}	0.11
Random nucleation kinetics model	−3,000	0.9951	−6.3	4.7×10^{-6}
Avrami–Erofeev model				
$n = 1.5$	1,900	0.9989	-3.6×10^{-2}	0.13
$n = 2$	1,000	0.9988	3.3×10^{-3}	1.6×10^{-2}
$n = 3$	100	0.9989	0.10	1.6×10^{-3}
$n = 4$	−400	0.9989	0.2	4.0×10^{-4}

E: activation energy, i: intercept, r: linear regression coefficient, A: frequency factor.

imental data. The results were equally poor when calculations were carried out in different conversion ranges with these models. Comparison of Table II(a) and II(b) also point out that the derivative mode of analysis of the dynamic data is more effective in discriminating between different models.

Results of Kinetic Modeling Using Data from Isothermal Experiments

Derivative Method of Analysis

For isothermal experiments, the value of the rate constant k is fixed; therefore, the numerical solution

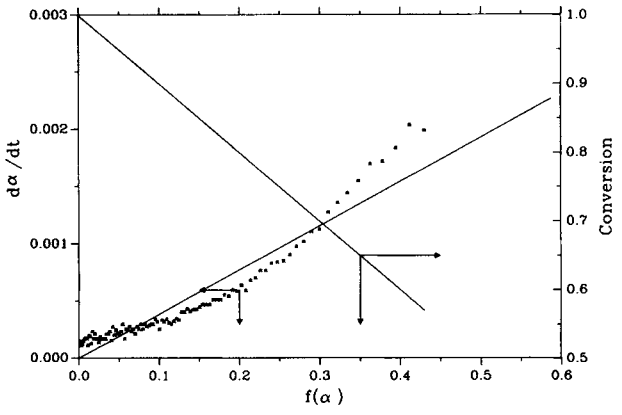

Figure 11 Derivative analysis of isothermal conversion data obtained at 450 K and 10 K/min approach to hold temperature. Homogeneous first-order kinetics model.

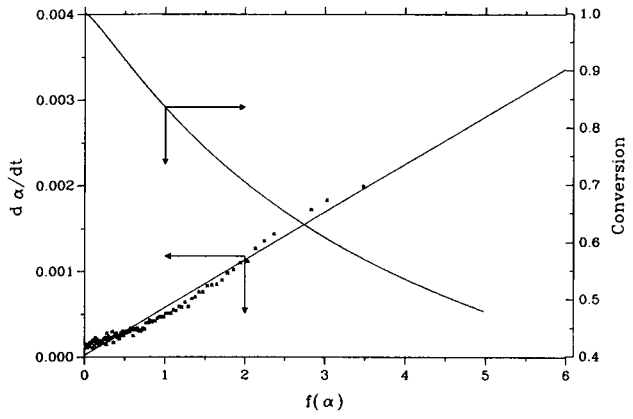

Figure 12 Derivative analysis of isothermal conversion data obtained at 450 K and 10 K/min approach to hold temperature. Jander kinetics model.

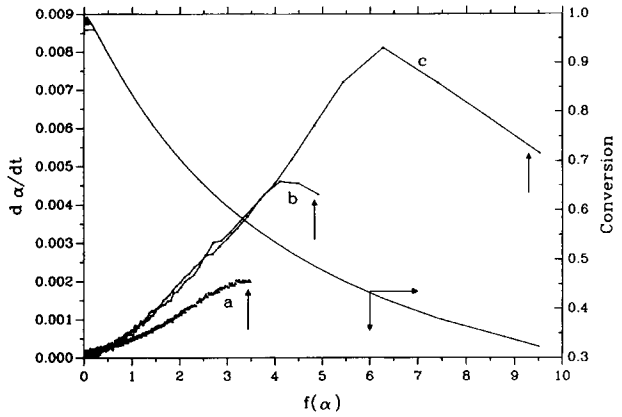

Figure 13 Comparison of derivative analyses performed on conversion data obtained for different rates of approach to isothermal hold temperature of 450 K: (a) 10 K/min; (b) 20 K/min; (c) 40 K/min approach.

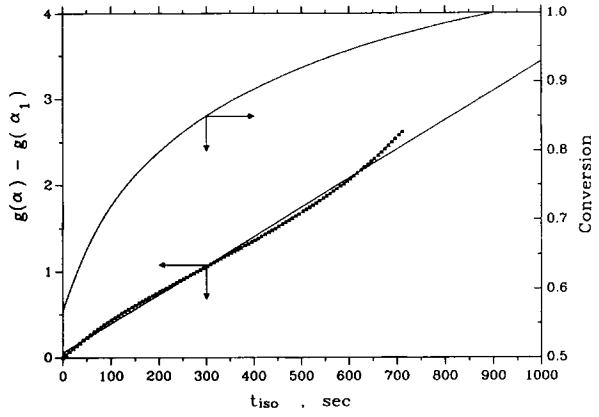

Figure 14 Integral analysis of isothermal data obtained at 450 K with 10 K/min approach to hold temperature. Homogeneous first-order kinetics model.

is straightforward. The results of using the homogeneous first-order reaction model to analyze data from isothermal experiments performed at 450 K are shown in Figure 11. This is a plot of $d\alpha/dt$ vs. $f(\alpha)$ and shows the actual data, the prediction represented by the thin straight line and the variation of the conversion with $f(\alpha)$. The results obtained using the Jander model is illustrated in Figure 12. Comparison of these figures show that the Jander model represents the data well.

Figure 13 shows the $d\alpha/dt$ values corresponding to isothermal data at 450 K that was approached at different heating rates, i.e., 10, 20, and 40 K/min. The values shown represent the data after isothermal conditions are first reached. These are marked with an arrow on each curve. However, during the changeover from dynamic heating to the isothermal hold mode, there is a transient region for stabilization. This is reflected by the initial irregularity of these curves at the lower conversion end. The $f(\alpha)$ values in this figure were determined using the

Table IV Derivative Analyses of Isothermal Data (10 K/min approach) (55–100% Conversion Range)

Model	r	k	i
First-order kinetics	0.9892	5.9×10^{-3}	-2.7×10^{-5}
Autocatalyzed kinetics model			
$n = 1, m = 1$	0.8945	6.5×10^{-3}	-1.2×10^{-4}
$n = 1, m = 2$	0.7296	8.5×10^{-3}	-1.2×10^{-4}
$n = 2, m = 2$	0.9719	2.7×10^{-2}	9.2×10^{-5}
1-Dimensional diffusion model ($n = 1$)	0.9739	4.4×10^{-3}	-2.1×10^{-3}
2-Dimensional diffusion model ($n = 1$)	0.9720	1.8×10^{-3}	-3.7×10^{-4}
Jander kinetics model	0.9812	4.9×10^{-4}	6.2×10^{-5}
Gintsling–Brounshtein model	−0.5091	-1.3×10^{-4}	8.7×10^{-4}
Contracting geometry model			
$n = 2$	0.8941	1.4×10^{-3}	-4.0×10^{-4}
$n = 3$	0.9289	1.0×10^{-3}	-2.2×10^{-4}
Random nucleation kinetics model	−0.9427	-3.8×10^{-3}	3.8×10^{-3}
Avrami–Erofeev model			
$n = 1.5$	0.9336	2.8×10^{-3}	-1.2×10^{-4}
$n = 2$	0.9027	2.1×10^{-3}	-1.7×10^{-4}
$n = 3$	0.8614	1.4×10^{-3}	-2.1×10^{-4}
$n = 4$	0.8360	1.0×10^{-3}	-2.3×10^{-4}

r: linear regression coefficient; k, rate constant; i, intercept.

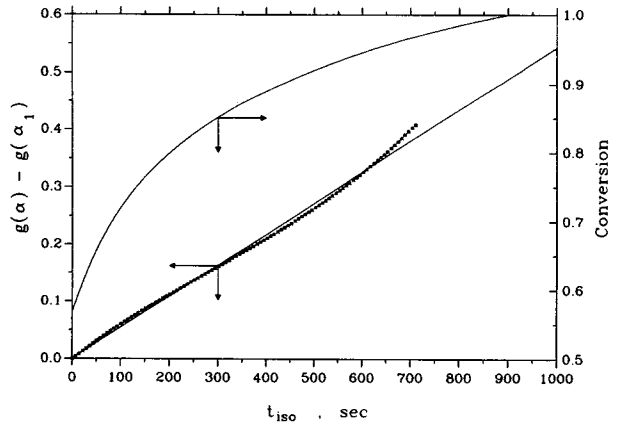

Figure 15 Integral analysis of isothermal data obtained at 450 K with 10 K/min approach to hold temperature. Jander kinetics model.

functional form corresponding to the Jander model. After the initial transient, the data appear to lie in a straight line passing through the origin, suggesting that the Jander model could be used to fit such data. The slopes become similar after the 20 K/min heating rate. It is not clear why the rate constant for the isothermal reaction depends on the rate of approach, except for the possible effect of different initial conversions.

The rate constants calculated from these analyses are presented in Table IV for all the models. The table shows the rate constants as well as the corresponding regression coefficients and intercepts. The homogeneous first-order reaction model and the Jander model have the highest regression coefficients and the lowest intercepts, which are the criteria for a good fit of the models to the experimental data. Even though some of the models, like the autocatalytic kinetic model and the one- and two-dimensional diffusion models, show a high degree of correlation, they fail to satisfy the second criteria, i.e., that the intercepts be close to zero.

Integral Method of Analysis

Integral analysis was performed on isothermal experiments conducted at 450 K and a 10 K/min approach. Figure 14 is a plot of $g(\alpha) - g(\alpha_1)$ against isothermal hold time (t_{iso}) for the homogeneous first-order model. The conversion profile of the experimental data is provided for better visual analysis. The crosses represent the experimental data and the straight line represents the model prediction. The data lie close to the straight line, indicating a good fit for the homogeneous first-order model. The Jander model was also tested for the same conversion data. The results are shown in Figure 15. The experimental data once again lies very close to the model prediction. These results corroborate the results obtained for the analyses of the dynamic data. Table V shows the rate constants as well as the cor-

Table V Comparison of Integral Analyses of Isothermal Data at 10 K/Min Approach (55–100% Conversion Range)

Model	r	k	i
First-order kinetics	0.9992	5.0×10^{-3}	6.3×10^{-2}
Autocatalyzed kinetics model			
$n = 1, m = 2$	0.9862	5.9×10^{-3}	0.2
$n = 1, m = 2$	0.9131	1.7×10^{-2}	2.0
$n = 2, m = 2$	0.9871	4.1×10^{-2}	0.7
1-Dimensional diffusion model $n = 2$	0.9867	1.0×10^{-3}	-8.8×10^{-4}
2-Dimensional diffusion model ($n = 2$)	0.9929	9.0×10^{-4}	-1.8×10^{-2}
Jander kinetics	0.9832	4.2×10^{-4}	-1.9×10^{-2}
Gintsling–Brounshtein model	0.9927	2.5×10^{-4}	-7.3×10^{-3}
Contracting geometry model			
$n = 2$	0.9904	8.4×10^{-4}	9.3×10^{-3}
$n = 3$	0.9953	6.8×10^{-4}	3.6×10^{-4}
Random-nucleation kinetics model	0.9201	2.8×10^{-3}	0.3
Avrami–Erofeev model			
$n = 1.5$	0.9970	2×10^{-3}	6.8×10^{-3}
$n = 2$	0.9923	1.6×10^{-3}	2.8×10^{-2}
$n = 3$	0.9842	1.1×10^{-3}	3.7×10^{-2}
$n = 4$	0.9789	8.8×10^{-4}	3.6×10^{-2}

r, linear regression coefficient; k, rate constant; i, intercept.

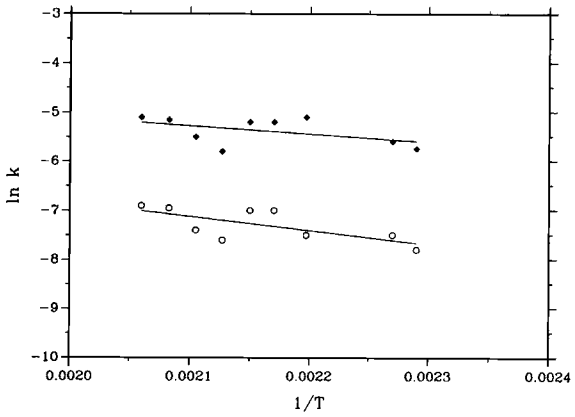

Figure 16 Rate constants vs. inverse temperature. Rate constants obtained from derivative analysis of isothermal data using the (♦) homogeneous first-order kinetics model and (○) the Jander kinetics model.

responding regression coefficients and the intercepts obtained from integral analyses using the various models. The homogeneous first-order reaction model and the Jander model have higher regression coefficients and lower intercepts. The analysis of dynamic data results based on analysis of the isothermal data indicates that the integral method of analysis does not have the ability to discriminate different models as clearly as does the derivative method of analysis.

Activation Energies from Isothermal Experiments

To obtain activation energies from isothermal experiments, a number of runs were performed at different temperatures. A plot of the rate constant with $1/T$ yields the value for the activation energy. Figure 16 illustrates this using rate constants obtained by performing derivative analysis of isothermal data with the first-order homogeneous model and the Jander kinetic model, respectively. The activation energies obtained are about 30 kJ/mol. These values are of the same order of magnitude (in the range of 20–40 kJ/mol) predicted from analyses of dynamic data shown in Table II(a). (An E/R value of 4500 corresponds to 38 kJ/mol.) However, in the literature, somewhat higher values have been reported.[6,10,22–24]

CONCLUSIONS

From the various analyses presented above using the derivative and integral procedures on data obtained from dynamic and isothermal experiments, it can be concluded that cure reactions can be represented by the first-order homogeneous reaction mechanism. Another model that also works well is the Jander 3-dimensional diffusion model. It is observed that beyond 30% conversion diffusional factors become especially significant as reflected by substantial decrease in the apparent activation energies after this conversion.

REFERENCES

1. J. M. Barton, in *Epoxy Resins and Composites I,* K. Dusek, Ed., Springer-Verlag, Berlin, 1985, p. 112.
2. B. A. Rozenberg, in *Epoxy Resins and Composites II,* K. Dusek, Ed., Springer-Verlag, Berlin, 1986, p. 115.
3. R. B. Prime, in *Thermal Characterization of Polymeric Materials,* E. A. Turi, Ed., Academic Press, New York, 1981, Chap. 5.
4. A. Knop and L. A. Pilato, *Phenolic Resins,* Springer-Verlag, Berlin, 1985.
5. A. W. Christiansen and L. Gollob, *J. Appl. Polym. Sci.,* **30,** 2279 (1985).
6. R. Kay and A. R. Westwood, *Eur. Polym. J.,* **11,** 25 (1975).
7. E. Kiran and R. Iyer, *TAPPI J.,* October (1993).
8. S. Chow and P. R. Steiner, *J. Appl. Polym. Sci.,* **23,** 1973 (1979).
9. V. A. Era, *J. Therm. Anal.,* **25,** 79 (1982).
10. C. R. Bhavsar, MS Thesis, University of Maine, Orono, 1989.
11. E. Koch, *Non-isothermal Reaction Analysis,* Academic Press, London, 1977, Chaps. 3 and 4.
12. C. H. Bamford and C. F. H. Tipper, Eds., *Comprehensive Chemical Kinetics,* Elsevier, New York, 1980, p. 22.
13. V. M. Gonzalez-Romero and N. Casillas, *Polym. Eng. Sci.,* **29**(5), 295 (1989).
14. H. Ng and I. Manas-Zloczower, *Polym. Eng. Sci.,* **29**(5), 302 (1989).
15. R. Iyer, MS Thesis, University of Maine, Orono, 1992.
16. P. W. K. Lam, H. P. Plaumann, and T. Tran, *J. Appl. Polym. Sci.,* **41,** 3043 (1990).
17. P. W. M. Jacobs and F. C. Tompkins, *Chemistry of the Solid State,* W. E. Garner, Ed., Butterworth, London, 1955.
18. A. Fevre and M. Murat, *J. Therm. Anal.,* **7,** 429 (1975).
19. M. Avrami, *J. Chem. Phys.,* **7,** 1103 (1939); **8,** 212 (1940); **9,** 177 (1941).
20. B. V. Erofeev and N. I. Mitskevich, in *Proceedings of the 4th International Symposium on Reactivity of Solids,* Elsevier, Amsterdam, 1961, p. 273.
21. K. L. Mampel, *Z. Phys. Chem. Abt. A,* **187,** 235 (1940).
22. Z. Katovic, *J. Appl. Polym. Sci.,* **11,** 95 (1967).
23. A. Sebenik, I. Vizovisek, and S. Lapanje, *Eur. Polym. J.,* **10,** 273 (1974).
24. C. G. Hill, *An Introduction to Chemical Engineering Kinetics and Reactor Design,* Wiley, New York, 1977, Chap. 12.

Received September 17, 1992
Accepted June 11, 1993